

Multiplex analysis of mass imaging data: Application to the pathology of experimental myocardial infarction

Han Shi¹ | Mary El Kazzi¹ | Yuyang Liu¹ | Antony Gao¹ | Angie L. Schroder¹ | Sally Vuong²  | Pamela A. Young³ | Benjamin S. Rayner² | Caryn van Vreden^{4,5} | Nicholas J. C. King^{4,5,6,7}  | Paul K. Witting^{1,7} 

¹Redox Biology Group, Discipline of Pathology, Faculty of Medicine and Health, Charles Perkins Centre, The University of Sydney, Sydney, New South Wales, Australia

²The Heart Research Institute, Faculty of Medicine and Health, The University of Sydney, Sydney, New South Wales, Australia

³Australian Centre for Microscopy & Microanalysis, Charles Perkins Centre, The University of Sydney, Sydney, New South Wales, Australia

⁴Immunopathology Group, Discipline of Pathology, Faculty of Medicine and Health, Charles Perkins Centre, The University of Sydney, Sydney, New South Wales, Australia

⁵Sydney Cytometry Facility and Ramaciotti Facility for Human Systems Biology, The University of Sydney, Sydney, New South Wales, Australia

⁶Marie Bashir Institute for Infectious Disease and Biosecurity, The University of Sydney, Sydney, New South Wales, Australia

⁷The University of Sydney Nano Institute, The University of Sydney, Sydney, New South Wales, Australia

Correspondence

Paul K. Witting, Discipline of Pathology, Faculty of Medicine and Health, Charles Perkins Centre, The University of Sydney, Sydney, NSW 2006, Australia.

Email: paul.witting@sydney.edu.au

Abstract

Aim: Imaging mass cytometry (IMC) affords simultaneous immune-labelling/imaging of multiple antigens in the same tissue. Methods utilizing multiplex data beyond co-registration are lacking. This study developed and applied an innovative spatial analysis workflow for multiplex imaging data to IMC data determined from cardiac tissues and revealed the mechanism(s) of neutrophil-mediated post-myocardial-infarction damage.

Methods: IMC produced multiplex images with various redox/inflammatory markers. The cardiac peri-infarct zone (PIZ) was determined to be up to 240 μm from the infarct border based on the presence of neutrophils. The tissue region beyond the infarct was defined as the remote area (RA). ImageJ was used to quantify the immunoreactivity. Functional assessments included infarct size, cell necro/apoptosis, total thiol assay and echocardiogram.

Results: Expression of damage markers decreased in order from the infarct area to PIZ and then RA, reflecting the neutrophil density in the regions. Concentrically spaced “shoreline contour analysis” around the cardiac infarct extending into the PIZ showed that immunoreactivity for damage markers decreased linearly with increasing distance from the infarct, concomitant with a decreasing neutrophil-myeloperoxidase (MPO) gradient from the infarct to the PIZ. Stratifying by concentric bands around individual MPO⁺-signal identified that the immunoreactivity of haem-oxygenase-1 (HO-1) and phosphorylated-p38 mitogen-activated protein kinase (pP38) peaked near neutrophils. Furthermore, spatial dependence between neutrophils and markers of cardiac cellular damage was confirmed by nearest-neighbour distance analysis. Post-infarction tissue exhibited declined functional parameters that were associated with neutrophil migration from the infarct to PIZ.

Conclusion: This image-based quantitative protocol revealed the spatial association and provided potential molecular pathways responsible for neutrophil-mediated damage post-infarction.

See related editorial: Sedmera D. 2022. Mass cytometry imaging in physiology *Acta Physiol (Oxf)*. e13822.

This is an open access article under the terms of the [Creative Commons Attribution-NonCommercial-NoDerivs](https://creativecommons.org/licenses/by-nc-nd/4.0/) License, which permits use and distribution in any medium, provided the original work is properly cited, the use is non-commercial and no modifications or adaptations are made.

© 2022 The Authors. *Acta Physiologica* published by John Wiley & Sons Ltd on behalf of Scandinavian Physiological Society.

Funding information

This work was conducted with grant support from the National Health and Medical Research Council of Australia (NHMRC Project APP1125392 to PKW).

KEYWORDS

imaging mass cytometry, myeloperoxidase, myocardial infarct, neutrophil, oxidative damage

1 | INTRODUCTION

Acute myocardial infarction (AMI) affects almost 3% of the global population.¹ The current paradigm for acute treatment is through the use of percutaneous coronary intervention to open the occluded coronary artery and achieve reperfusion of the ischaemic myocardium. However, this practice is associated with ischaemia/reperfusion injury,^{2,3} which can stimulate host tissue damage, remodelling of the myocardium and negatively impact the clinical outcome.³ One pathological process that has become a focus is the acute infiltration of the neutrophils into the infarct area and peri-infarct zone (PIZ) after AMI. This PIZ is also termed the penumbral region surrounding the primary infarct region, and is also referred to as the area-at-risk, where viable cardiomyocytes can be subject to neutrophil-mediated host damage.^{4,5} For example, myeloperoxidase (MPO), an enzyme expressed by all neutrophils, is enzymatically active producing the potent oxidant hypochlorous acid (HOCl) in the myocardium post AMI; the MPO level is linked to the frequency of adverse events including cardiac dilatation, ventricular dysfunction^{6,7} and cardiac arrhythmia.⁸

The deleterious effects of neutrophil-derived myocardial damage are potentially accelerated by enhanced oxidative stress and post-translational protein modification leading to enzyme dysfunction and the promotion of pro-inflammatory signalling cascades^{4,9} in the affected cardiomyocyte. However, the exact molecular pathways, biochemical changes and how best to monitor these changes to elucidate the key pathogenic mechanism(s) post-AMI remain unclear. Whether opportunities exist for therapeutic advances based on targeting immune cells is now a focus for current research.¹⁰

Multiplex immunohistochemistry by imaging mass cytometry (IMC) can facilitate the elucidation of molecular pathways involved in cellular damage and the resultant compensatory response due to the fact that this novel research tool allows the simultaneous detection of multiple antigens in one tissue section.¹¹ The technique of IMC ablates and vaporizes tissue that is labelled with heavy metal-conjugated antibodies, which are then detected by time-of-flight mass spectrometry, generating high-resolution multiplex images (Figure S1). Presently, application of this technique is primarily limited to immunological and cancer pathologies, which takes advantage of IMC by employing myriads of cell surface markers to identify unique cell populations through co-registration.

The study of organ pathology and pathophysiology, however, relies on elucidating the interplay between subcellular markers that do not necessarily colocalize. To date, there is no protocol readily available that explores the spatial relationship among a variety of markers from a heterogenous group of cells beyond their colocalization. Development of such an innovative protocol that can be easily integrated into a routine image analytical procedure will greatly extend the use of IMC to the physiology and pathology fields.

The primary aim of this work was to develop a robust but time-efficient analytical protocol and associated workflow to ascertain an array of protein changes linked to pro-inflammatory damage in inflamed tissue, taking account of the spatial relationship of a range of biological markers in order to infer their biological roles, using the freeware, ImageJ (<https://imagej.nih.gov/ij/>). Consequently, our secondary aim was to determine whether this protocol can independently reveal, for the first time, the extent of neutrophil-mediated damage to myocardial tissue in a rat AMI/reperfusion model by assessing the spatial relationship between neutrophils and a range of markers of cellular damage and activation within this setting, including neutrophil marker MPO,¹² the inflammatory mediator tumour necrosis factor alpha (TNF), the pro-inflammatory markers phospho-P38 mitogen-activated protein kinase (pP38) and NF- κ B-p65 phospho-ser276 (pP65), the oxidative damage marker malondialdehyde (MDA), acute phase antioxidant enzyme haem oxygenase-1 (HO-1) and glutamate cysteine ligase catalytic subunit (GCLC), the accompanying rate limiting enzyme in the synthesis of reduced glutathione, both integral parts of the nuclear factor erythroid 2-related factor 2 (Nrf2)-mediated antioxidant response.

2 | RESULTS

2.1 | Histology, MPO activity and confirmation of antibody specificity in the infarcted rat heart

The presence of a myocardial infarction was confirmed by haematoxylin and eosin (H&E) histology in rats assigned to the AMI group (Figure 1A) compared with the surgical sham. The histological sections of myocardium also guided the selection of a region of interest (ROI) for IMC imaging such that the ROI contained the infarct, PIZ and RA

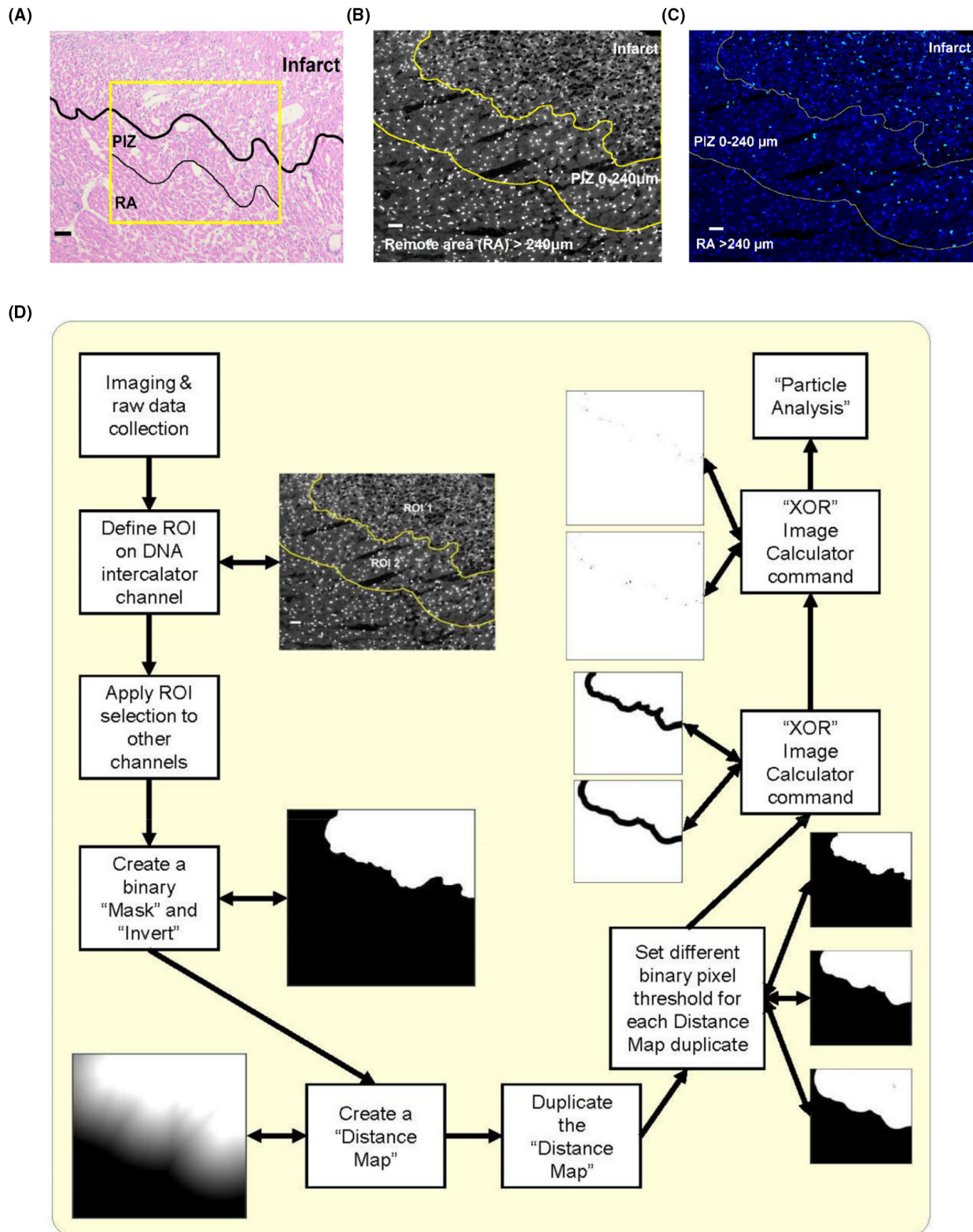


FIGURE 1 Areal definition and shoreline contour analysis workflow. (A) H&E histology of the myocardial infarct (above the black line). The yellow square indicates an example of ROI selection. Scale bar = 100 μm . (B) Designation of the Infarct area, PIZ and RA via DNA intercalation channel. Scale bar = 50 μm . (C) Neutrophils (MPO^+ immunoreactivity, cyan) in the infarct and PIZ but not RA. Hence the location of neutrophils determines that the PIZ extends up to 240 μm from the infarct border. Scale bar = 50 μm . Navy immunoreactivity: nuclei. (D) Analysis workflow; details in the methods Section 4.7

regions as shown in the representative region outlined by the yellow square. Under the “nuclear channel” for IMC images where the nuclei were marked with a DNA intercalator (Figure 1B), the infarct area on the top right was precisely identified based on the lack of cellular structural integrity of the cardiomyocytes and the irregular shapes of the nuclei. Consistent with the rapid recruitment of innate immune cells following acute myocardial damage,¹³ IMC detected infiltrating neutrophils within the infarct and in the region immediately surrounding the infarct. The area 0–240 μm from the infarct border was designated the peri-infarct zone (PIZ) and the area >240 μm from the infarct border denoted the remote area (RA), where the border between the infarct and PIZ and the border between PIZ and RA were highlighted in yellow. Such designation is because IMC immunoreactivity assessment of the myocardium indicated the presence of large numbers of infiltrating neutrophils located within the infarct zone, with fewer neutrophils in the peri-infarct zone and rarely present beyond 240 μm from the infarct border (Figure 1C).

This method of regional division was subsequently used to facilitate the recognition of potential associations between neutrophils and other protein targets in the same pathologically relevant myocardial zones. By contrast, the inflammatory response in samples obtained from the surgical sham was located only at the outermost border of the myocardium, closest to where the pericardium was damaged with the appearance of normal myocardial predominating in hearts from this treatment group (data not shown).

In order to first validate the use of metal-conjugated antibodies in this IMC study, the individual immunoreactivity of all antibodies employed was compared with corresponding specific immunofluorescence signal intensities recorded using standard fluorescence microscopy. A selection of antibodies that target markers relevant to AMI has previously been reported to be elevated in ischaemia/reperfusion injury^{4,14–19} in order to elicit the evidence of different aspects of neutrophil–MPO-mediated damage during the acute phase of AMI. Specifically, we imaged MPO (Figure S2A), HO-1 (Figure S2B), GCLC (Figure S2C), pP38 (Figure S2D), pP65 (Figure S2E), TNF α (Figure S2F) and MDA (Figure S2G). These representative images demonstrate the immunofluorescence labelling (top, labelled “IF”) and the corresponding metal-conjugated immune labelling (bottom, labelled “IMC”); identical pattern for each of the antibodies studied, used as a single-label and mass-analysed at high (20 \times) and low (10 \times) resolution for comparison. Overall, we observed near identical patterns of tissue labelling for both fluorescence and metal-labelled antibodies, with comparable subcellular localization and overall comparable punctate morphologies within the various regional zones of the heart tissue assessed.

2.2 | IMC multiplex analyses of myocardial tissues

Application of IMC to rat heart tissue sections produced multiplex images with specific patterns of immunoreactivity for each of the protein markers used (Figure 2). The transition boundaries between the infarct and PIZ and between PIZ and RA are denoted by the yellow lines in the representative micrographs (Figure 2 panels A–K). Figure 2A showed MPO and the pro-inflammatory marker, phosphorylated P38 (pP38—Figure 2A–C red signal), which displayed immunoreactivity throughout the infarct, PIZ and RA regions. In subsequent high-powered images, pP38⁺ immunoreactivity was clearly discernible in both the nucleus (as evident by the overlap of blue nuclear signal in Figure 2B, arrowed) and cytoplasm in many of the cells in the infarct region, PIZ and RA (Figure 2A,B and Figure S2D), yielding a pattern suggestive of MAPK activation and nuclear translocation. Interestingly, almost all MPO⁺ immunoreactivities were also positive for pP38, with a consistent pattern of co-localization for these two labels (Figure 2C). Since all neutrophils express MPO,¹² this pattern strongly indicates MAPK activation in both neutrophils and host cardiomyocytes as a post-damage response. This notion is further supported by the observations that differential size of the pP38 staining between the MPO⁺ and MPO[−] cells suggests expression in cells of different morphology (ie, a different cell type—in this case cardiomyocyte vs neutrophils), as does the polymorphic appearance of the neutrophil (MPO⁺) blue-staining nuclei. Colocalization of MPO⁺ and nuclear immunoreactivity was assessed using the “Plot Profile” function in ImageJ, which measures the grey scale intensity along the lines of interest (Figure 2D, yellow lines). A representative plot of the grey scale values is shown in Figure 2E. The fact that every single peak of MPO⁺ immunoreactivity has a corresponding peak nuclear intensity indicates that the detected MPO⁺ immunoreactivity is of cytoplasmic origin as opposed to exocytosed granules.

Contrary to the expectation that damage markers would be highly expressed within the infarct region, pP65 immunoreactivity was detected primarily outside the infarct region, with little evidence of Nf κ B transcriptional activation detected within the infarct zone (Figure 2F); this may reflect the degree of rapid necrosis occurring in the primary infarct zone limiting cells from mounting this targeted molecular response. By contrast, examination of the antioxidant response element, HO-1, revealed that this enzyme formed a punctate cytoplasmic localization pattern mainly within the infarct region (Figure 2 panels G, K), with HO-1 immunoreactivity observed to a lesser extent within the PIZ. Images shown in Figure 2H–K demonstrate co-registration of MPO, TNF, GCLC and MDA immunoreactivity. Unlike

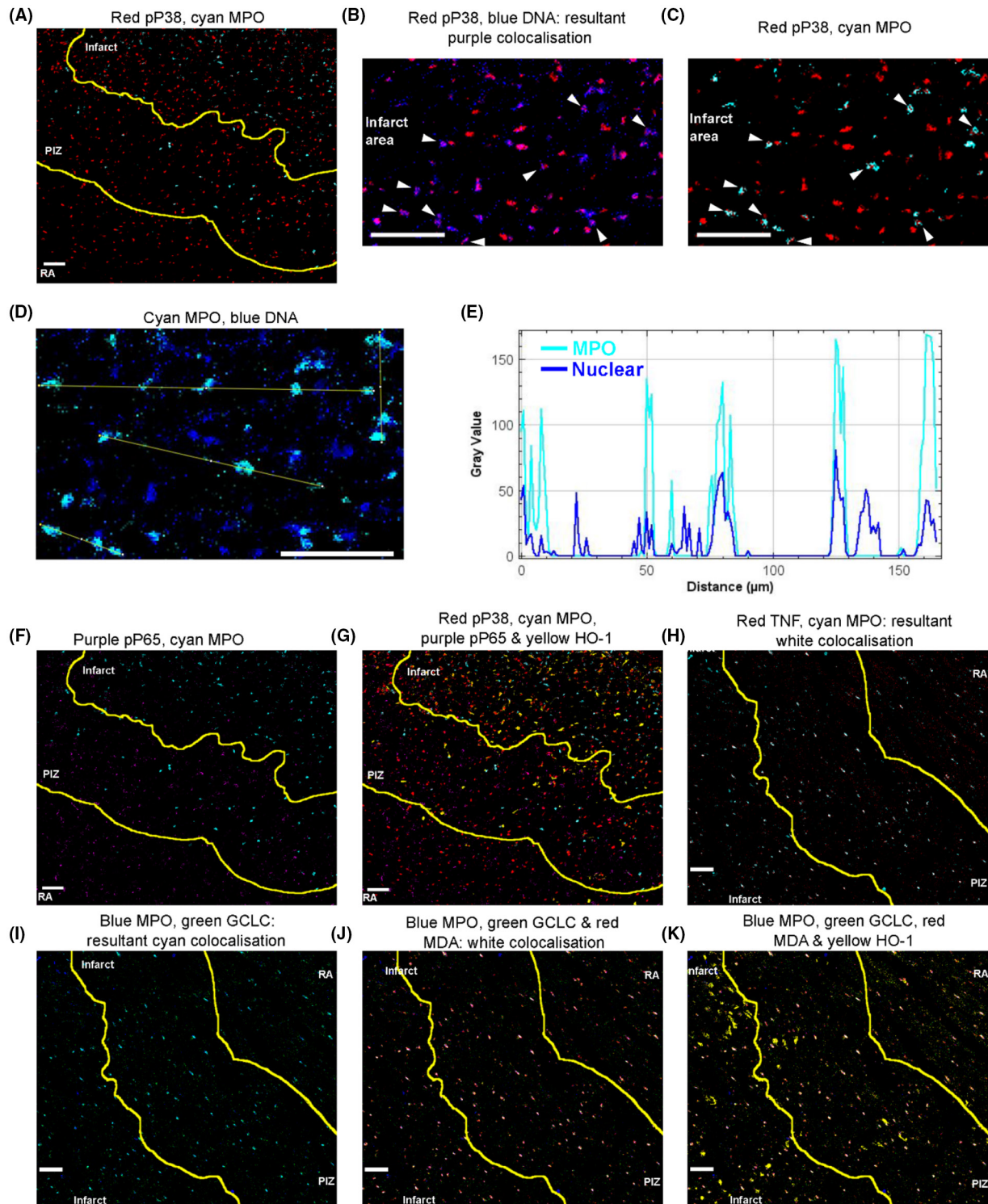


FIGURE 2 Multiplex imaging data. (A) Immunoreactivity of p38 and MPO in the same tissue section and field of view as [Figure 1B](#); the transition from the infarct to PIZ and from PIZ to RA denoted by the yellow lines. (B) Co-registration of p38 and nuclear staining in the infarct (arrow heads). (C) Immunoreactivity of p38 immediately adjacent to that of MPO (arrow heads). (D) An example of line-profile assessment where the intensity was measured under the MPO and nuclear channel along the yellow lines. (E) Representative line-profile data. (F-K) Multiplex imaging of immunoreactive signals. Scale bars = 50 μm

HO-1, these other protein biomarkers co-labelled with the MPO⁺ neutrophil signal indicating neutrophils were the primary source of pro-inflammatory TNF signalling and

the likely central cause of oxidative stress that elicited subsequent host cellular damage and antioxidant responses in the vicinity of these infiltrating cells.

2.3 | Regional comparison of relative signal intensities

Since a majority of MPO⁺ immunoreactivities were located within the infarct and PIZ, the RA portion of heart tissue was employed as the internal control for the subsequent analyses to aid in the spatial assessment of neutrophil-related myocardial damage. The mean percentage area of MPO immunoreactivity decreased from ~0.6% in the infarct zone to ~0.4% in the PIZ and further still to a significant decrease down to ~0.2% in the RA zone (Figure 3A), consistent with the decrease in the number of infiltrating neutrophils across these regions of the affected myocardium. The same relationship was also observed using signal frequency, which decreased from ~4.5 in the infarct zone to ~2.5 in the PIZ and to ~0.8 in the RA zone, and using InDen, which decreased sequentially from ~5 in the infarct to ~3.5 and finally ~0.3 within RA (Figure S3A,D). Similarly, the immunoreactivity for the antioxidant response element HO-1 and the pro-inflammatory marker pP38 decreased progressively from the infarct to PIZ to RA (Figure S3B,C,E,F), and also decreased significantly from PIZ to RA when normalized against the immunoreactivities in the infarct area (Figure 3B,C). This association between neutrophils and biomarkers of cellular response/activation reinforced the pathological potential of inflammation in the PIZ region in ongoing myocardial damage. This was not observed in the RA, where the myocardium remained free of both cellular infiltration and evidence of cardiomyocyte activation/damage, as demonstrated by the lack of MPO immunoreactivity in the RA region as shown in Figures 2A and 3E.

2.4 | Infarct border shoreline contour analysis

Using concentric contour bands that are 40 μm wide, a “shoreline contour” analytical approach was adopted to analyse the spatial distribution of biological markers in PIZ at varying distance from the border of the infarct. Figure 3D,E outlines the concept of shoreline analysis when selecting channels that specify the nuclear⁺ and MPO⁺ immuno-fluorescent responses, respectively. Using the three independent analytical methods outlined above, measurement of the markers within bands revealed a potential link between the myocardial damage/activation shown post-AMI and the extent of infiltrating neutrophils. For example, using the values in the infarct and RA as references, the signal frequency and InDen for MPO immunoreactivity within a given shoreline band decreased linearly as bands moved progressively away from the defined infarct border, diminishing by ~75%-80% in the most distal band measured (Figure 3F and Figure S4 for exemplar

linear regression analyses). The same staggered decrease in MPO immunoreactivity holds true for measurement of percentage area (Figure S3G). This differential distribution reflects a graded infiltration of neutrophils into the infarct and the PIZ, as represented graphically, with the MPO signal diminishing in the overlaying shoreline contours as they reduce in number away from the infarct zone (Figure 3H). Similarly, the HO-1 and pP38 immunoreactivity also decreased linearly with increasing distance from the border of the infarct with all three measurements (compare Figure 3 panels F, G; Figures S3G,H and S4 for linear regression), which maps closely with a similar decline in MPO immunoreactivity. Of note, the majority of linear regression analyses showed a strong ($R^2 > 0.8$) moderate ($R^2 > 0.6$) relationship between density of the biomarkers and distance from the infarct border (Figure S4), signifying their spatial distribution.

Next, this relationship between redox/inflammatory markers and distance was correlated against the relationship between MPO and distance. Statistically significant correlation ($P < .05$) was shown to exist between MPO and HO-1 expression as well as between MPO and pP38 expression, as assessed by the extent of signal frequency (Figure 4A,B), indicating the number of individual cells expressing the relevant biomarkers follow the same gradient in the PIZ. When both the intensity of each individual immunoreactive centre and the total area of these centres were taken into account through application of the InDen measurement, strong ($R^2 > 0.85$) and highly significant ($P < .01$) correlations were determined between MPO and HO-1 expression as well as between MPO and pP38 expression (Figure 4C,D). However, the correlation between areas alone, ie, corresponding comparison of the percentage area, did not reach statistical significance although this remained a moderate trend (Figure 4E,F). This does not mean that the percentage area measurement is inferior to the InDen approach, as aforementioned strong and significant correlation exists between individual biomarkers and distance from the infarct border (Figure S4). Rather, the presence of anomalies (labelled 80 μm in Figure 4E,F) indicated the limitation of traditional correlation: exaggeration of deviation from the line of best fit. This is where correlating the slightly lower-than-best-fit values of MPO percentage at 80 μm (Figure S4G) and higher-than-best-fit values of HO-1 and pP38 percentage area at 80 μm (Figure S4H,I) from simple biomarker-distance correlation produced outlier data that can potentially skew the linear relationship. Overall, this accumulated data support the hypothesis that infiltrating neutrophils in the myocardium mediate host damage in the PIZ and highlight the need for an independent, confirmatory assessment, as described below.

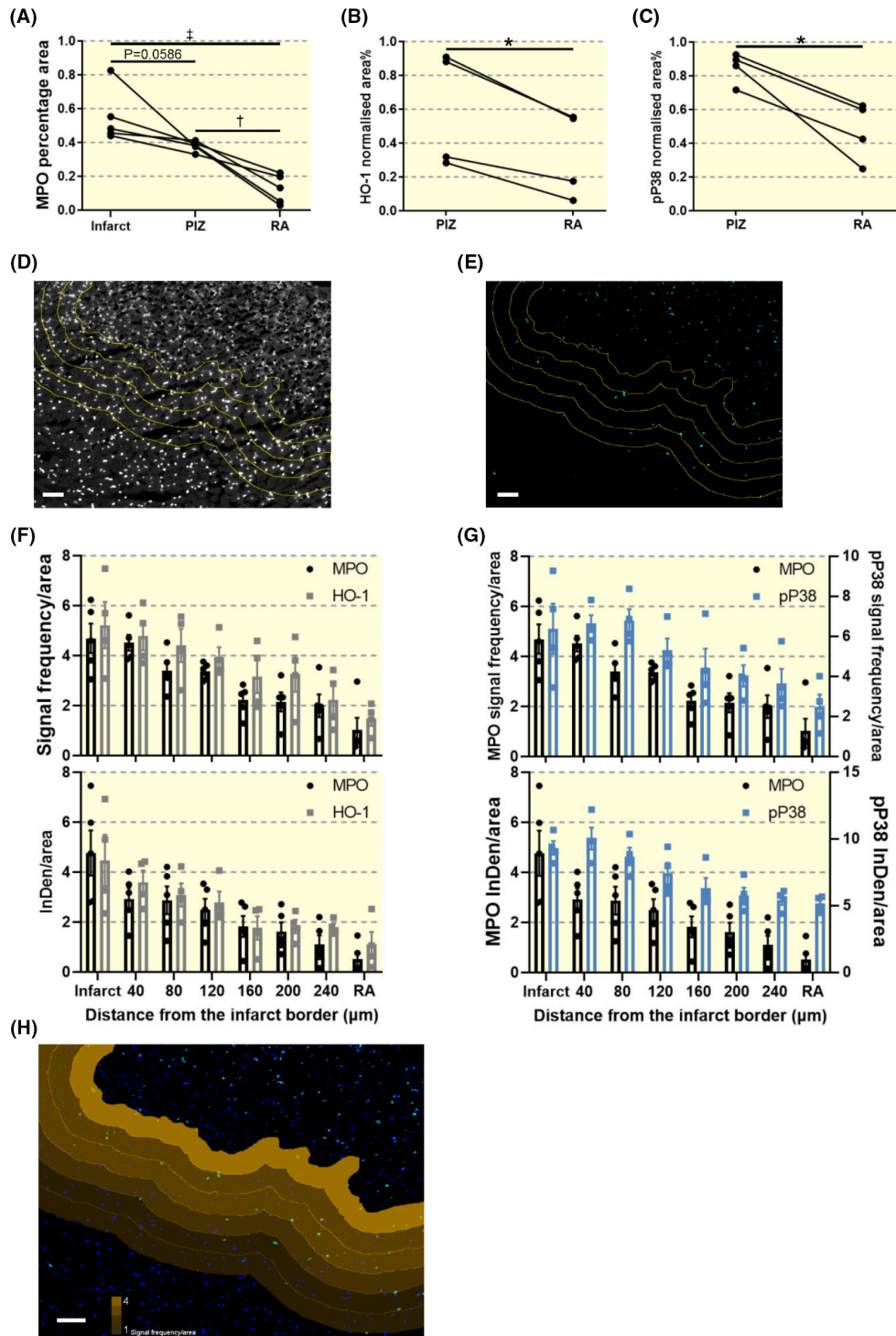


FIGURE 3 Multiplex image spatial analysis. (A) MPO⁺ immunoreactivity decreased in order from the infarct, PIZ to RA. (B, C) Percentage areal occupation (area%) of HO-1 and pP38 in PIZ and RA divided by their corresponding values in the infarct zone. (D, E) Rationale for the shoreline analysis: concentric shoreline contour bands from the infarct area overlaid on the nuclear (D) and MPO (E) channels. (F, G) HO-1⁺ and pP38⁺ immunoreactivity quantified via signal frequency, ie, the counts of signals within each ROI, and InDen, the integrated density of each pixel over the area of all immunoreactive signals. (H) Graphical representation of MPO InDen. Scale bars = 50 μm

2.5 | Neutrophil border shoreline contour analysis

Despite the relatively large number of neutrophils, there was no obvious association between percentage area and

distance from each neutrophil (Figure 5C,D). This suggests neutrophils did not directly contribute to the expression levels of a majority of the damage markers monitored here, which most likely arose from the initial myocardial ischaemia due to experimental coronary vessel occlusion.²⁰⁻²²

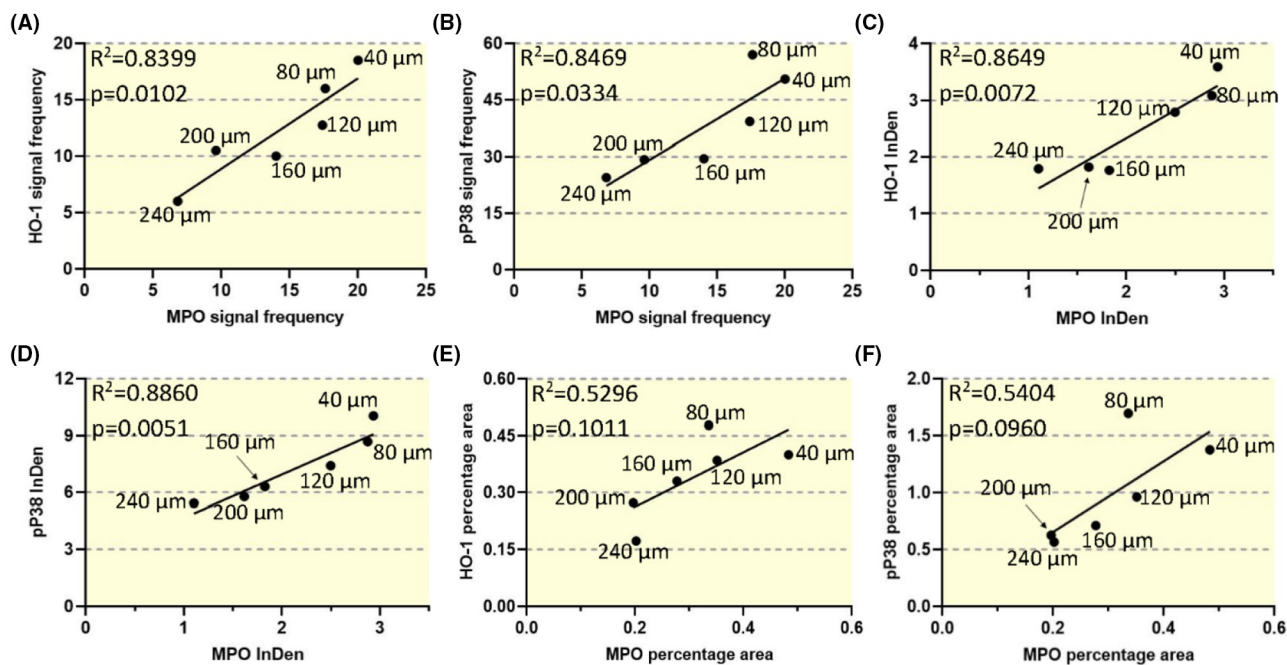


FIGURE 4 Correlations between redox/inflammatory markers and MPO based on distance from the infarct border. Linear regression for the redox/inflammatory markers HO-1/pP38 expression and the distance from the infarct border correlated against the linear regression for MPO expression and its distance from the infarct border (data taken from Figure S4). Significant correlation indicates that neutrophils contribute to HO-1/pP38 expression consistently at different shoreline bands, highlighting their likely pathological role

However, upon inspection of the trend from each biological replicate, as indicated by each line that connects the individual values, there are subtle decreases in peak responses when comparing data at 50 and 20 μm distance. This phenomenon was also observed using the InDen approach for analyses (Figure S3I,J). Given the size of cardiomyocytes, a peak within the band 10-20 μm from a neutrophil is expected, but whether neutrophils contributed to those damage biomarkers requires an assessment with a method that can differentiate the effects from acute myocardial ischaemia; a process that is presently outside the scope of this study. Regardless, the low levels of pP38 detected at 10 μm (Figure 5D) is most likely due to exclusion of pP38 immunoreactivities that overlap with MPO signals, with the latter signal stemming primarily from the neutrophils accumulating in the tissue post-AMI.

2.6 | Nearest-neighbour distance (NND) for interaction analysis

Adjusting the parameters for the NND analysis allowed the programme to filter out non-specific immunoreactive signals (Figure S5). From the series of markers examined here, the antioxidant response element HO-1 showed the greatest degree of spatial interaction with MPO in the PIZ, as evidenced by the different shapes of observed and model fit (Figure 6B, blue and green lines, respectively)

compared with context (red) with determination of a high interaction strength value = 36 (Figure 6B). The observed NND distribution demonstrated a higher probability density (blue curve) than context when the distance was between 5 and 25 μm , indicating some of the HO-1⁺ immunoreactivities within 25 μm of each MPO⁺ immunoreactivity might stem from neutrophil-mediated activities. This is consistent with the peak HO-1⁺ immunoreactivity density being within the shoreline band 20 μm from each neutrophil (Figure 5D). However, the distinction should be made that for NND, only the nearest HO-1⁺ signal for each MPO⁺ signal was taken into account, while the shoreline bands around each MPO⁺ signal map incorporated all the HO-1⁺ immunoreactivity. Therefore, the discrepancy between a significant MPO-HO-1 NND spatial interaction and a trend in the shoreline bands, which did not reach statistical significance may be because a significant proportion of HO-1 expression stems from the initial ischaemia due to acute tissue hypoxia²³ rather than the sequence of reperfusion injury and subsequent neutrophil recruitment. This means that a portion of the HO-1 signal detected within the concentric bands around individual neutrophils stems from the initial hypoxic insult to the myocardium and, therefore, does not display any spatial inter-relationship with neutrophils, overall rendering a non-significant trend.

Within the primary infarct region, which is the major site of myocardial injury, a less strong but

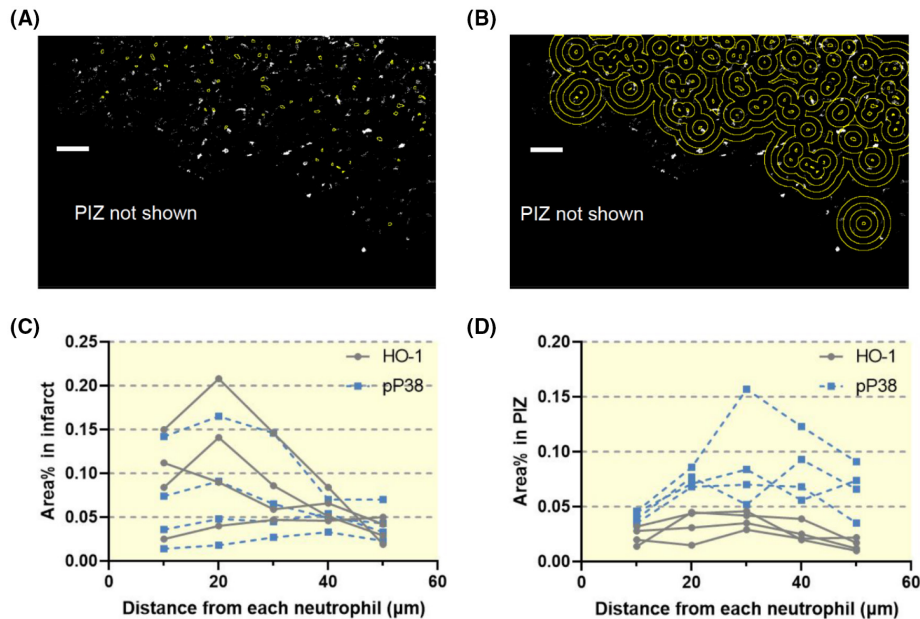


FIGURE 5 Neutrophil border shoreline analysis. (A) The signals of neutrophils outlined in yellow and then overlaid on white HO-1 channel. (B) Concentric shoreline bands of 10 μm distance were drawn around the outlines of individual neutrophils identified by the MPO⁺ immunoreactivity. Panels (C, D) Percentage Area (Area)% occupied by HO-1⁺ and pP38⁺ immunoreactivity in each shoreline contour band, respectively, was plotted against the corresponding distance away from each neutrophil-MPO⁺ signal identified. Scale bars = 50 μm

significant MPO-HO-1 NND interaction was observed with strength = 6.2 (Figure S6A). Combining the degree of HO-1 spatial interaction with MPO in all zones (infarct, PIZ and RA) produced a weaker but significant spatial relationship with interaction strength value = 4.9 (Figure S6B); this decreased interaction was attributed to the lack of association in the RA where HO-1 is present (Figure 3B) as a result of global oxidative stress while neutrophils rarely migrated beyond the limit of the PIZ. The spatial interaction between MPO and pP38 was also confirmed in the PIZ (Figure 6C), infarct (Figure S6C) and all areas combined (Figure S6D) with interaction strength values >1 . The MPO-pP38 NND association was comparable to the MPO-HO-1 association but consistently less strong for any given or combined area. One reason is that, similar to HO-1, a greater proportion of pP38 expression might be attributed to the initial ischaemic insult^{24,25} as observed in the global presence of pP38 expression (Figure 2A) and its relatively high density (Figure 3C) in the RA. Statistical analyses of the corresponding interaction curves demonstrated a significant interaction ($P < .01$ for MPO-pP38 in the infarct and $P < .001$ for the remainder of tissue regions) for all the above NND analysis, validating the assessment of interaction strength and further supporting the presence of an interaction between MPO⁺ neutrophils and the other biomarkers in the damaged myocardium.

As mentioned previously, pP65 immunoreactivity was primarily located in the RA, with only moderate pP65

immunoreactivity in the PIZ, while NF κ B activation (as measured by phosphorylation of P65) was rarely detected in the infarct zone (Figure 2F). The small sample size of pP65 in the PIZ resulted in a poorly defined (undulating) signal for the MPO-pP65 NND distribution curve (Figure 6D). When considering the PIZ region alone or all three regions combined, no spatial interaction was indicated as the estimated NND curve clearly overlapped with the context curve and the interactive strength values were only marginally above 0 (Figure 6E); furthermore, there was no statistical significance ($P > .05$) between the interaction curves in any of the regions, again suggesting that transcriptional activation of NF κ B was independent of MPO and potentially a consequence of global oxidative stress brought on by the ischaemic insult.

2.7 | Relationship between measures of myocardial neutrophil-MPO and altered cardiac function after experimental heart attack

Next, the footprint of myocardial neutrophil-MPO was assessed for correlations with biomarkers of the pathophysiology of the AMI. Production of hypochlorous acid (HOCl) by MPO in biological tissues yields the protein oxidation marker 3-Chlorotyrosine (3-Cl-Tyr). The ratio of 3-Cl-Tyr:total tyrosine levels is widely used as an *in vivo* marker of MPO activity. Liquid chromatography-mass spectrometry revealed

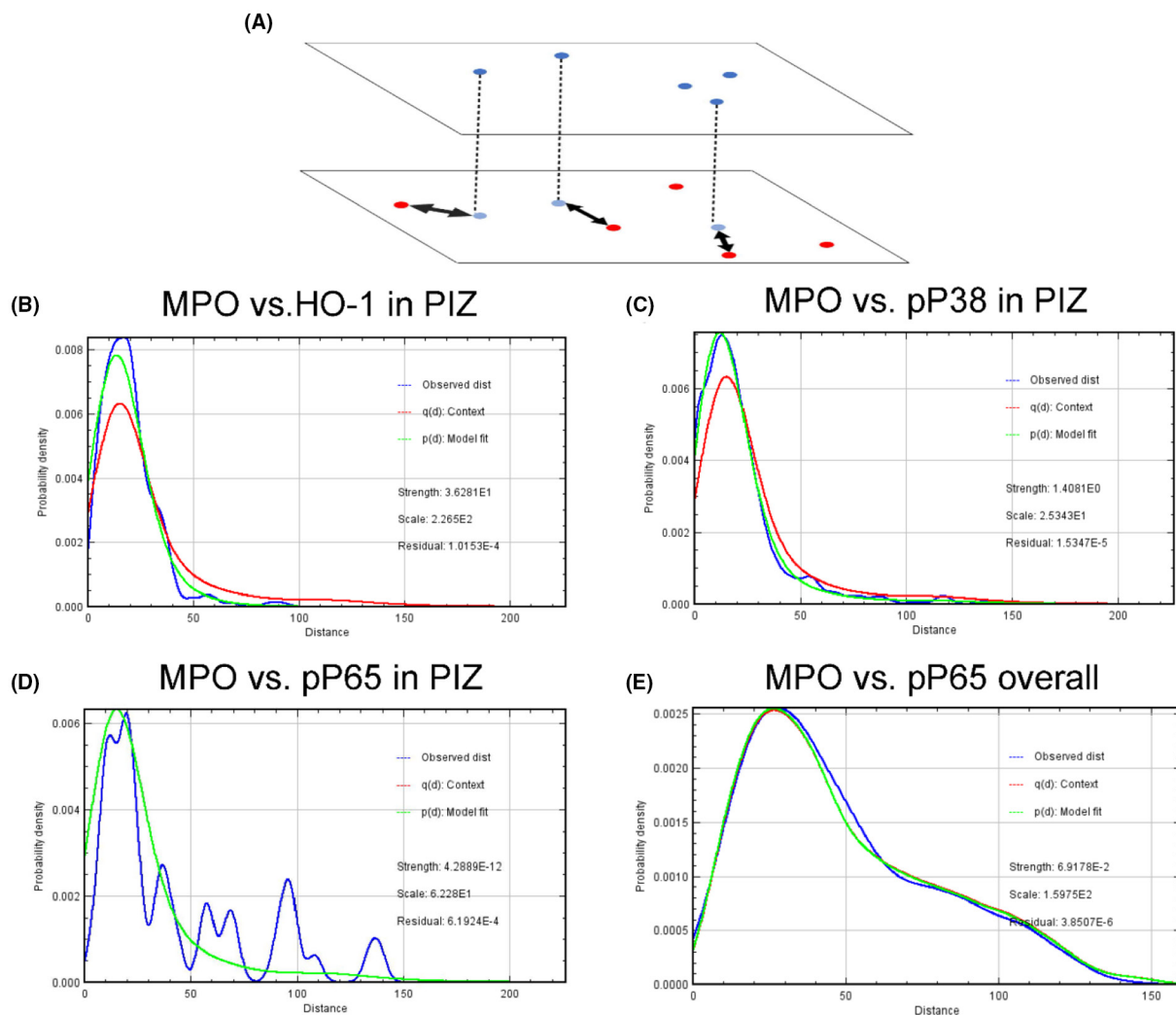


FIGURE 6 Nearest-neighbour distance (NND) analysis. (A) Rationale of NND. Blue dots are mapped onto a group of red dots. The distance between the nearest non-overlapping blue dot for each red dot is NND. (B) NND distribution of between each MPO⁺ and HO-1⁺ immunoreactivity in PIZ. “Context” (red): NND distribution from two random, independent groups of dots. “Strength”: the strength of spatial interaction (0 is absence association, 0-1 is indeterminant, >1 is strong association). (C) NND distribution between MPO⁺ and pP38⁺ immunoreactivity. (D, E) A lack of spatial association between pP65⁺ and MPO⁺ immunoreactivity

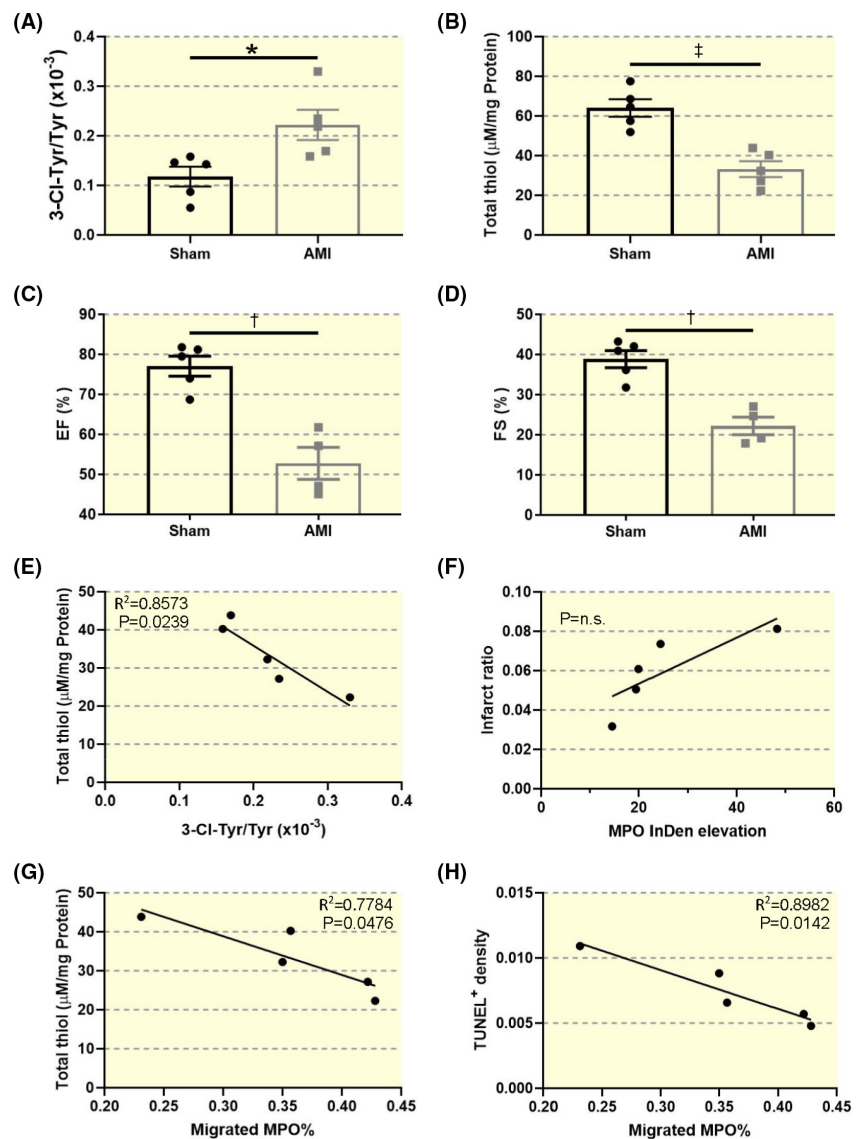
a significant increase in 3-Cl-Tyr levels in the AMI group relative to the surgical sham (Figure 7A), consistent with active MPO (from infiltrating neutrophils) damaging proteins within the infarct region and PIZ. Of note, the basal 3-Cl-Tyr levels from the sham group was due to opening of the pericardium during the sham surgery, which resulted in low-level inflammation and hence fewer infiltrating neutrophils. On the other hand, total thiol levels, which represent the combination of low-molecular weight reduced glutathione (GSH) and protein thiol residues, were significantly reduced in the AMI group (Figure 7B). This reflected the increased global oxidative stress that can be attributed to ischaemia, followed by reperfusion and consequently the activity of neutrophil-derived MPO.

Cardiac function can be represented by two parameters of echocardiology, ejection fraction (EF) and fractional

shortening (FS), both of which measures the cardiac muscle contractility. Thus, functional data were obtained from a parallel study where the experimental AMI and reperfusion was induced using the same protocol vs sham. Under these identical experimental conditions, both EF (Figure 7C) and FS (Figure 7D) decreased at 28 days post-AMI, demonstrating the deleterious effects on cardiac output.

These various biomarkers provided data to conduct a series of point-by-point analysis. For example, plotting total thiol levels against the corresponding 3-Cl-Tyr levels for each individual cardiac specimen (Figure 7E) yielded a strong and statistically significant linear relationship. This correlation suggests that MPO activity is potentially a major contributor to enhanced oxidative stress in damaged cardiac tissue 24 hours post-AMI, which alters tissue levels of the reduced thiols. In

FIGURE 7 Functional assessment. (A) The marker of MPO activity, 3-Cl-Tyr:Tyr ratio was increased in the AMI group. (B) Total thiol levels were lower in the AMI group. (C, D) Ejection refraction (EF) and fractional shortening (FS) were decreased in the AMI group at 28 days post-AMI in a parallel study. (E) Total thiol levels decreased linearly with increasing 3-Cl-Tyr:Tyr ratios. (F) The Infarct ratio was not mathematically related to MPO InDen elevation. (G, H) Total thiol levels and TUNEL⁺ density were negatively associated with migrated MPO%



addition, the size of the infarct area in each specimen was calculated as the infarct ratio, ie, the area of the infarct divided by the total area of the cardiac cross section. By treating the RA as the internal control for each individual heart, the level of MPO InDen in the infarct was normalized by the level of MPO InDen in the corresponding RA to determine the relative increase of MPO immunoreactivity for each specimen; this parameter was termed “MPO elevation” (Figure 7F) and was reflected by the degree of neutrophil infiltration histologically in the same heart tissues. The infarct ratio was not mathematically related to MPO elevation, but the infarct ratio increased with increasing MPO elevation as indicated by a monotonic distribution. This is completely consistent

of involvement of the neutrophils determines the final infarct size.²⁶ However, MPO elevation only accounts for the presence of neutrophils in the infarct, and its levels were not associated with other biological parameters such as total thiol levels that are determined from the combined infarct, PIZ and to a lesser extent the RA tissue. After reperfusion of the infarct, neutrophils extravasate and entered the infarct area that is supplied by the occluded vessel and then migrated outward to the PIZ. Since neutrophils also damage the viable cardiomyocytes in the PIZ, which can ultimately lead to adverse cardiac remodelling and inferior cardiac function,⁴⁻⁶ the percentage of the neutrophils that have achieved migration to this region was defined as follows:

$$\text{Migrated MPO \%} = (\text{MPO}^+ \text{ signal PIZ} - \text{MPO}^+ \text{ signal RA}) / (\text{MPO}^+ \text{ signal INF} + \text{MPO}^+ \text{ signal PIZ} - \text{MPO}^+ \text{ signal RA}) * 100,$$

with the formation of the infarct occurring primarily during the ischaemic phase of AMI, while the degree

where INF, PIZ and RA represent the MPO InDen levels in the infarct, PIZ and RA, respectively. Migrated

MPO% showed a strong correlation with total thiol levels (Figure 7G), suggesting that a higher percentage of migrating neutrophils are activated to yield MPO-derived oxidants that are associated with a lower total thiol level. As indicated above, the total thiol level was measured using the cardiac tissue homogenate derived from the infarct area, PIZ and to a lesser extent RA. However, since the infarct consists of necrosed tissue with low thiol levels due the prior ischaemic damage, we interpret that the measured total thiol level is more representative of remaining thiols within viable cells and connective tissues from the PIZ. Therefore, the association between a decreased thiol level and migrated MPO% is concordant with the secondary oxidative damage caused by activated neutrophils in the PIZ independent of the initial ischaemic damage.

Finally, assessment of the degree of cell death in the infarct region with Terminal deoxynucleotidyl transferase (TdT) dUTP Nick-End Labelling (TUNEL) yielded a negative association between TUNEL⁺ density and migrated MPO%. This strong negative correlation is interpreted as lower a number of neutrophils in the infarct contributing to a low rate of cell death with a majority of the loss in cardiomyocyte viability accountable in the initial ischaemic phase of AMI. Once again, this outcome is consistent with the literature where neutrophil activities can lead to cell death and eventually increase the infarct size.²⁷ The division of the three areas (infarct, PIZ and RA) and quantification of neutrophil migration, however, emphasized the fact that neutrophils exert local effects, with ongoing tissue damage limited to their relative density and proximity in the tissue region.

3 | DISCUSSION

To the best of the authors' knowledge, this is the first study that applies IMC in the pathology of acute myocardial inflammation resulting from experimental AMI in rodents. Here, we presented an efficient and economical workflow analysis for assessing non-colocalizing immunoreactivities, consisting of regional analysis, shoreline contour analysis and NND analysis, which can be applied on any multiplex image data set and easily integrated into the image analysis routine using ImageJ. The analysis utilizes the "Distance Map" function from ImageJ which allows distance-mapping of the objects in the image by pixels, and the full analytical protocol requires less than half an hour per image. This analysis workflow can be applied to any multiplex set of tissue antigens analysed by IMC. A strength of this approach is identification of the spatial relationships between the non-colocalizing antigens that extend beyond simple signal co-registration.

The current model of myocardial infarction consists of two phases of damage, ie, the initial ischaemic phase and the reperfusion phase. Clinically, the ischaemic phase occurs spontaneously and is difficult to develop targeted treatment, while the reperfusion phase consists of standard percutaneous coronary intervention without preventative measures against reperfusion damage. Neutrophil-MPO, an important contributor to the post-reperfusion myocardial damage, is responsible for post-AMI ventricular dysfunction^{6,7} and arrhythmia,⁸ and represents one of the ideal therapeutic targets as MPO inhibition can be administered while recruitment of the neutrophils to the infarct occurs at the 6-24 hours post-reperfusion time frame. Hence this study aims to extend the understanding of the molecular pathways downstream of MPO activities using MPO as a reference point in the spatial analyses.

In this study, regional analyses and shoreline contour band analyses revealed that the total levels of damage marker expression correlate with the expression of MPO⁺ immunoreactivities, ie, the number of infiltrating neutrophils. However, one potential explanation is that this correlation is because both MPO⁺ immunoreactivity and damage marker immunoreactivity correlate with their distance from the border of the infarct. Therefore, NND analysis was introduced as a method independent of the location of the antigens relative to the infarct. Unlike traditional immunoreactivity analysis which takes into account every signal, NND analysis has the advantage that it is able to determine spatial dependence based on the single "nearest neighbour." This is extremely important in the pathology of AMI where there are two phases of damage marker expression. For example, a small percentage of pP38 expression that arises from neutrophil activities at 6-24-hour post-reperfusion could be indistinguishable from the pP38 expression due to the initial ischaemic phase and reperfusion damage. Here, NND analysis has shown that a proportion of the pP38⁺- and HO-1⁺-immunoreactivities is spatially related to neutrophils, especially when these protein epitopes are within 25 μ m of each neutrophil. In contrast, pP65⁺ immunoreactivity is not related to neutrophils. Combining these analyses and pathological role of neutrophils, it can be deduced that neutrophil activities are responsible for the elevated expression of damage markers and exacerbate the inflammatory and oxidative damage in the myocardium after AMI. However, the causal relationship can only be verified by depletion studies (eg, using MPO gene deletion in mice).

Subsequent results from combining functional assessments and IMC multiplex data support the hypothesis of neutrophil-mediated damage in the PIZ. Compared with surgical shams, AMI-reperfusion leads to increased MPO activities, more severe oxidative damage and worse cardiac function. Importantly, the correlation between total thiol

levels and 3-Cl-Tyr suggested that MPO activity was responsible for exacerbation of oxidative stress. Furthermore, as measured by migrated MPO%, the presence of neutrophils was associated with increased cell death locally. Taken together, these associations determined here provides an insight into the struggle between damage to local tissue and host defence/response aimed at enhancing myocardial viability²⁷; a diminished capacity to recover viable myocardium may be linked to progression to heart failure.²⁸

3.1 | Immunoreactivity expression in myocardial infarction

In our 24 hours-post AMI model, the use of MPO as the marker for neutrophils is not affected by the presence of macrophages or monocytes that are recruited to the myocardium at later stages. In the case for monocytes, these do not express MPO²⁹ but require induction³⁰ to produce significant levels of MPO. Regardless, minimizing the number of cell markers reduces the chance of interference. While the pattern of ischaemia-reperfusion injury reflects the clinical scenario, it can, to some extent, confound the study of biomarkers due to their differential temporal expression. For example, MAPK pP38 can be upregulated in the first phase in response to ischaemia^{24,25} and in the second phase due to MPO activity.^{8,31} Similarly, HO-1 can be upregulated in myocardial hypoxia²³ (phase one) via transcriptional activation of hypoxia-inducible factor-1 (HIF-1).^{23,32} Therefore, analyses aiming to establish the relationship between neutrophils and biomarkers necessarily need to discriminate between potential dual impacts associated with temporally separated primary and secondary expression in AMI. Coupling co-localization, shoreline analysis and NND analysis, with tissue demarcation into three distinct regions (infarct, PIZ and RA), offer the power to detect biomarkers related specifically to neutrophils that are recruited to these regions. This is because these methods rely on the spatial distribution of biomarkers, which differentiates the global expression in phase one from the sporadic expression clustered around neutrophils.

Notably, MPO immunoreactivity co-registered with the pro-inflammatory marker TNF, the oxidative damage marker, MDA, and the acute-phase antioxidant enzyme, GCLC. Neutrophils express TNF to induce inflammation,³³ but increased expression of the redox markers, GCLC and MDA, is likely to represent direct damage to nearby cardiomyocytes as a result of MPO activity yielding the potent oxidant hypochlorous acid (HOCl). Upon degranulation, MPO catalyses the production of HOCl (and other hypohalous acids³⁴) that

are implicated in host tissue damage. Clearly, HOCl is the major and most potent oxidant species generated by neutrophils in appreciable amounts within inflamed biological tissues.²⁰ The two-electron oxidant, HOCl, reacts with a range of biomolecules,²¹ and this high level of non-specific reactivity towards biological reductants²² confines its diffusion to only within 1 μm of the site of generation. Therefore, the redox markers may be tightly associated with MPO activity and reflect MPO-mediated damage, which explains the colocalization of MPO-, TNF-, MDA- and GCLC-immunoreactivities. Hence, these markers were not selected for contour shoreline mapping because the primary application of this technique was designed for non-colocalizing signals (an advantage over standard approaches that are limited to colocalizing outputs).

3.2 | The myocardial response to oxidative stress

With increased oxidative stress, nuclear factor (erythroid-derived 2)-like 2 (Nrf2), a master transcription factor, binds to the antioxidant response cis-element (ARE) in the promoters that enhance the expression of antioxidant enzymes, including HO-1 and GCLC.^{35,36} The resulting cardioprotective effects are absent in Nrf2-knockout mice.¹⁷ The activation of Nrf2-GCLC/HO-1 pathway was also described in response to hypochlorous acid challenge in a dose-dependent manner in vitro, which promotes cell survival.^{37,38} Although the IMC analyses here could not report the expression of Nrf2 due to a lack of suitable antibody for rat tissue, the intimate spatial association between neutrophils and antioxidant enzymes GCLC and HO-1 demonstrated here is suggestive of a cellular response to MPO-mediated HOCl production. Such a paradigm is significant to the PIZ where the cardiomyocytes remain viable after AMI, unlike the necrotic cells in the infarct, and thus may be subject to further damage and cardiac remodelling. Clinically, the viability of the peri-infarct zone is a powerful predictor of post-AMI mortality,³⁹ while polymorphism in antioxidant enzymes, such as GCLC, is associated with poor outcome after myocardial infarction.¹⁴ Our data also suggest that future interventions aimed at inhibiting this form of damage may lead to the identification of new therapeutic strategies in the post-AMI phase of recovery.

Studies have reported elevated expression of NF- κ B pP65 that mediates myocardial damage in the same AMI model and time point of 24 hours post-infarction.¹⁹ Here we noted that pP65-immunoreactivity (as a surrogate for NF- κ B activation) was rarely detected in the infarct zone, while pP65-immunoreactivity was more evident in the PIZ

and RA. This result runs contrary to the expectation that the infarct represents the centre of damage and necrosis and should express highest levels of acute damage markers. This discrepancy might stem from the different time course of NF- κ B expression inside and outside the infarct zone with the cellular response to acute damage occurring prior to the time these hearts were harvested. In support of this notion, pP65 expression, signifying translocation of NF- κ B to the nuclear envelope of the activated cells, reportedly occurs with a window of 10-20 hours post stimulation.⁴⁰ Since damage in the infarct area starts during the initial ischaemic phase and neutrophil migration to the damaged myocardium occurs approximately 4-6 hours after reperfusion and continues for the next 24-48 hours¹³ then it is feasible that heart retrieval at 24 hours post-surgery may have missed the pP65 expression window for within-infarct detection. Nevertheless, the data obtained here suggest that pP65 expression is independent of infiltrating neutrophils and this cellular response is likely due to other stimuli including localized oxidative stress due to impaired oxygenation.⁴¹

3.3 | Translational relevance

Given the pathological relevance of neutrophils we observed and its association with adverse post-AMI events such as cardiac dilatation, ventricular dysfunction⁶ and arrhythmia,⁸ it follows that MPO may be a useful therapeutic target. In fact, a recent study has reported that MPO inhibition improves ventricular function and remodelling after experimental AMI.⁷ Notably, the detrimental effects of MPO reactivity is not limited to AMI, but a variety of conditions featuring acute immune cell infiltration or chronic inflammation, as MPO inhibition appeared beneficial in murine disease models including chronic obstructive pulmonary disease,⁴² bowel inflammation⁴³ and stroke.⁴⁴ Taken together, these findings highlight the pathological significance of MPO-mediated tissue damage.

3.4 | Limitations and future work

Limitations of the current study include the following: (a) IMC is a novel technique that requires antibody conjugation with heavy metals. Therefore, the antibody-reactivity to the required tissue and specificity need to be established and validated in each case. Antibodies that cross-react over several animal species may not produce robust immunoreactivities (such as the case of the polyclonal antibody raised against Nrf2) and, (b) Expansion of this method to couple with corresponding cardiac tissue from MPO knock-out (KO) mice and/or specific pharmacological inhibitors of MPO activity

are necessary to identify downstream pathways subsequent to MPO activation and provide strong evidence for the causality of MPO-mediated post-AMI adverse cardiac remodelling and the deterioration of cardiac function.⁶

3.5 | Conclusion

In conclusion, the current study described a spatial relationship analysis protocol (refer to general workflow shown in Figure 1) for non-colocalizing immunoreactivities that can be applied in any multiplex imaging techniques, especially in the application of IMC. Through combining this protocol and signals that co-register, our results suggest that neutrophil activities are associated with redox/inflammation damage within and around the infarct following AMI. The advantage of this protocol is that it can reveal spatial interactions independently without a requirement for depletion studies.

4 | MATERIAL AND METHODS

4.1 | Animal model

All animal work was performed with compliance to ARRIVE guidelines of animal experimentation, with ethical approval from the local SLHD AEC (2017/032). Male Wistar rats (~150-200 g body weight) were purchased from Animal Resources Centre (Perth, WA, Australia), transported and acclimated for 7 days prior to random assigned into two groups designated as the surgical SHAM (n = 5) and AMI (n = 5) group(s). Where required, rats were anesthetized with 5% isoflurane/in oxygen carrier gas then intubated and maintained on 2%-3% isoflurane using a ventilator with close monitoring; depth of anaesthesia in each rat was confirmed with repeated toe pinch. To avoid the eye drying during the procedure, rats were treated by gentle application of Paralube[®] prior to surgery. Next, the chest was shaved to expose the skin in the upper left region. Antiseptic was applied (Betadine[®]) in the upper through to mid rib area with a clean swab, and anaesthesia was applied by local injection (Lidocaine, 0.5% v/v solution 3 minutes before surgery, maximum volume 0.2 mL). Experimental AMI/R was induced by exposing the heart between the 4th and 5th rib and left coronary artery ligation (30 minutes) performed according to the established protocol⁴⁵ with reperfusion (removal of ligation) and recovery of each animal taking place in isolated cages with an operating heat mat for 24 hours. Where required, hearts were collected for subsequent analysis with euthanasia performed by anaesthesia overdose (5% v/v isoflurane).

4.2 | 3-Chloro-tyrosine (3-Cl-Tyr) quantification

The modified amino acid 3-Cl-Tyr is a specific biomarker for MPO activity as HOCl chlorinates tyrosine residues on proteins. Levels of 3-Cl-Tyr were quantified by liquid chromatography–mass spectrometry according to the published protocol.⁴⁶ Detection of 3-Cl-Tyr and unmodified tyrosine and corresponding labelled internal standards was performed on a Shimadzu LCMS8050 coupled with Nexera X2 LC system.

4.3 | Histological assessment of myocardial architecture

Haematoxylin and eosin (H&E) staining was performed using parallel thin-tissue sections of 5 μm , taken from formalin-fixed (10% v/v) and paraffin-embedded hearts. A ZEISS Axio Scan.Z1 Slide Scanner was employed for high-resolution scanning of the entire tissue section. The size of the infarct and the cross-sectional area of the myocardium was measured by the number of pixels on ImageJ and compared at 50 μm from the pericardium. The infarct ratio was calculated from the infarct size divided by the cross-sectional area.

4.4 | Antibodies and immunofluorescent staining

Eight commercial, polyclonal antibodies (detailed in Table S1) that target myeloperoxidase and other specific markers of oxidative stress and inflammatory response were used to perform singleplex immunofluorescence microscopy using sequentially sectioned heart tissue. Slides were deparaffinized, rehydrated and underwent antigen retrieval using a decloaking chamber (Biocare Decloaking Chamber™ Pro) with sodium citrate buffer pH 6.0. Endogenous peroxidase activity was blocked by addition of 3% v/v hydrogen peroxide diluted in Tris-buffered saline (100 mM) containing Tween 20 (0.5% v/v Tween 20; referred to as TBST) for 10 minutes, followed by blocking with 3% w/v bovine serum albumin dissolved in TBST for 40 minutes at 22°C on the bench.

To validate the specific reactivity of the antibodies in rat heart tissue, primary antibodies were diluted in a preparation of antibody diluent (TBST + 0.05% w/v BSA, 0.05% v/v Triton-X) and incubated with the tissue section (1 hour, 22°C; final dilution ranging 1/200–1/100 v/v; refer to Table S1) before incubation with the appropriate secondary antibodies (1 hour, 22°C) (DAKO Envision HRP-conjugated anti-rabbit K400311 or Alexa

Fluor anti-mouse A-11020; final dilution 1:250 v/v). Where HRP-conjugated secondary was used, OPAL620 fluorophore (Perkin Elmer FP1498) was used to visualize the immune positive signal. Finally, all slides were counterstained with 4',6-diamidino-2-phenylindole (DAPI) spectral (Perkin Elmer FP1498). A Zeiss Axio Scope 4305 fluorescent microscope was used for imaging, and Zen Blue 2.5 software was used for image capturing and subsequent processing.

4.5 | Antibody conjugation and antigen labelling for imaging mass cytometry

A “Maxpar Antibody Labelling Kit” (Fluidigm) was used to conjugate a unique heavy metal element that is absent in the tissue to each of the antibodies (Table S1; protocol from Fluidigm, file PRD002 Version 11). Briefly, an antibody cocktail containing all eight conjugated antibodies each at the optimal concentration, as demonstrated in single-plex immunofluorescence (Table S1), was incubated with tissue sections (12 hours, 22°C). Iridium DNA Intercalator (Fluidigm 201192) in 1:400 v/v TBST was incubated (5 minutes, 22°C) to stain nuclei within the myocardium.

4.6 | IMC signal regional analysis

All subsequent image analysis was performed using the freeware “ImageJ” from the NIH (<http://imagej.nih.gov/ij>). Three independent approaches were used to quantify a specific label signal, including (a) “percentage area” which corresponded to the percentage area occupied by a specific label signal within a designated total areal region of the myocardium; (b) “signal frequency,” which employed a count of contiguous signal pixels in a given myocardial area/region, used to denote the number of immunoreactive centres detected; and (c) “Integrated Density” (InDen) which multiplies the area of each immunoreactive signal and its density (on a scale of 0–255) within a given myocardial area/region, measured directly by using ImageJ. An expanded description of the protocol for IMC signal regional analysis has been included in the supplemental methods with details of all parameters employed.

Based on the DNA-intercalator channel which shows the cytoplasmic structure and locations of nuclei, as shown in Figure 1B, the border of the infarct was drawn using the “Freehand Selection” function from ImageJ to create a ROI. The ROI was then overlaid onto other channels for comparison of signal frequency inside and outside of the infarct. The “Distance Map” function (explained in detail

in the next section) was used to outline the area ranging progressively further away from the identified infarct border (at distances 0–240 μm), defined as the PIZ. The remaining imaged tissue more than 240 μm from the infarct border was defined as the remote area (RA). Finally, the percentage total area occupied by specific immunoreactivities was measured by “Particle Analysis” for the distinct regions: infarct, PIZ and RA, respectively.

4.7 | Shoreline contour analysis—mapping to the infarct border

A “shoreline contour” analytical approach was adopted to allow a rigorous spatial analysis of biological markers. Thus, beginning with the closely mapped edge of the outer infarct border, ie, the beginning of the PIZ, a series of concentric shoreline contour bands, each 40 μm in width, was progressively projected outwards onto the tissue image with each contour stepped away from the infarct. To achieve this goal using freeware ImageJ (NIH; <http://www.imagej.nih.gov/ij/>), we developed the workflow using the “Distance Map” function (Figure 1D). First, the infarct region was identified based on cellular morphology under the nuclear channel (Figure 1B), and it was enclosed by the “free hand” tool to become ROI. Under the “binary mode,” the ROI selection was applied onto other channels that showed immunoreactivities to create a “mask” over the infarct region using “Mask” function, resulting in the infarct region being black (RGB 255,255,255). Then, the entire image was “inverted,” with the infarct region being white (RGB 0,0,0) and the rest of the image black. Next, the conversion from pixels and binary intensity to micrometres was achieved using “Distance Map” function. This created an area that decreased its intensity by 1 for every micrometre further away from the ROI. This image was duplicated, and different intensity threshold values, ie, shades of grey, were set to create masks of the same shape but different sizes. Specifically, to achieve a band width of 40 μm , the threshold values were set at RGB (40,40,40) or higher, in increments of 40 each time up to RGB (240,240,240), thus forming the shorelines extending from the infarct border up to 240 μm away. The “XOR” formula under “Image Calculator” function was run between the above masks to create concentric bands, which were used to select the immunoreactivity within each band using “AND” formula. Finally, the signal identified was quantified using a “Particle analysis” approach.

As in the previous section, the three independent methods were performed to quantify the immunoreactivities of the specific signals within each segmented band. Each shoreline band had the same area and therefore the signal frequency was used for linear regression as shown

in Figure S4. However, since the values in the infarct and RA were added for reference in the data shown in Figure 3F,G, the signal frequency was then divided by the corresponding ROI area to validate these comparisons.

4.8 | Shoreline analysis—mapping the border surrounding infiltrating neutrophils

The same process of shoreline analysis was applied around each neutrophil (Figure 5A,B). The location of neutrophils and their borders were defined by combining MPO⁺ immune reactivity and the DNA intercalation channel. “Freehand Selection” was used to draw an ROI around each neutrophil and all ROIs were combined (Combine ROI function) before procession to the same workflow of overlaying ROIs onto other channels as described above. For example, representative images shown in Figure 5A illustrate HO-1- (white)labelled immunoreactivity with overlaying borders of neutrophils (yellow) from the same tissue section. Next, concentric shoreline contour bands (10 μm separation) were drawn around each individual neutrophil (Figure 5B) in order to demonstrate a potential association with the damage markers. Refer to supplemental methods for detailed parameters.

4.9 | Nearest-neighbour distance (NND) analysis

Subsequent to the shoreline contour analysis, a second independent interaction analysis was performed using the MosaicIA function plugin for ImageJ to conduct an NND analysis,^{47,48} which maps one assigned group of immunoreactive signals onto another and calculates the NND between immunoreactive centres (eg, shown schematically by the two-headed arrows linking immune reactive centres, Figure 6A). The observed distribution of NND was then compared with a range of mathematical equations representing different types of spatial interactions^{47,48} and the best fit was plotted against the observed data for comparison. Spatial dependence is indicated when the shape of the observed NND distribution is similar to the mathematical model fit, but differs from “Context” that is defined as the NND distribution from two hypothetical, independent groups of immunoreactive centres. The strength of dependence was reported by the plugin where a value of 0 indicates no interaction; a designation of 0–1 represents a weak or no interaction while a value >1 strongly indicates the presence of nearest neighbour interaction. The plugin then performed a statistical test to assess the likelihood of interaction for each of the paired of proteins by ranking

the observed NND distribution against *K* Monte-Carlo samples of point distributions with the cut-off of 0.95 K -th in the ranking.^{47,48} An expanded detailed description of the protocol has been included in the supplemental methods.

4.10 | Assessment of total myocardial thiol levels

Levels of reduced glutathione (GSH) was measured spectrophotometrically as reported previously⁴⁹ by reaction of homogenates with 5,5'-dithio-bis (2-nitrobenzoic acid) (DTNB, 1.5 mg/mL) at 412 nm. Serial dilutions of GSH in potassium phosphate EDTA buffer (KPE) were used to create a standard curve. Cell homogenates were prepared in 0.1 M KPE (pH 7.5) before being loaded into a COSTAR 96 well flat bottom plate. A mixture of DTNB: glutathione reductase solution (1:1 ratio) was added to each well for 30 seconds followed by β -NADPH; absorbance was read at 412 nm every 30 seconds for 2 minutes.

4.11 | TUNEL staining of non-viable cell levels

Cell necrosis and apoptosis in myocardial tissue sections were detected using a TUNEL fluorometric kit (Promega, NSW, Australia). The slides were deparaffinized in xylene and rehydrated through a series of graded alcohols, fixed in paraformaldehyde in PBS (4% v/v), washed in PBS and permeabilized in 20 μ g/mL proteinase K (22°C; 10 minutes). Subsequent to further fixation in paraformaldehyde (4% v/v), the slides were incubated with equilibration buffer (22°C; 10 minutes) then with rTdT incubation buffer [90% Equilibration Buffer, 10% Nucleotide Mix, 2% rTdT Enzyme (37°C; 1hour)]. Reaction was stopped by immersion in 2xSSC, and nuclei were counterstained by 1:600 Spectral DAPI (PerkinElmer, USA) in TBST. ZEISS AXIO SCOPE upright fluorescent microscope (Zeiss, NSW, Australia) was used for imaging. The TUNEL⁺ density was calculated by the measured intensity of fluorescence normalized against the section area on MetaMorph[®] image analysis software (version 7.6; Molecular Devices, San Jose, CA, USA).

4.12 | Echocardiogram assessment of the cardiac function

A transthoracic echocardiogram in the parasternal short-axis position at the mid-ventricle level was performed at 4 weeks post-AMI using rats from a parallel study that underwent the same AMI-reperfusion protocol. A SonoSite Edge II Ultrasound System (Bothell, WA, USA) with a

HSL25x/13-6 MHz transducer (Fujifilm Sonosite, Bothell, WA, USA) was used for echocardiogram assessment. Left ventricular end-systolic diameter (LVESD) and left ventricular end-diastolic diameter (LVEDD) were measured in M-mode. Three independent recordings were performed in triplicate for each individual rat, and their mean values were used to calculate the fractional shortening (FS) and ejection fraction (EF) according to the following formulae:

$$FS(\%) = [(LVEDD - LVESD)/(LVEDD)] \times 100,$$

$$EF(\%) = [(LVEDD^3 - LVESD^3) / (LVEDD^3)] \times 100.$$

4.13 | Statistical analysis

All statistical analysis except NND analysis was performed on GraphPad Prism 7.04. Data sets for SHAM and AMI cohorts were confirmed to be normally distributed as follows: comparison of the 3-Cl-Tyr:Tyr ratio from the sham/AMI group and all regional comparison were adjudged normal by the Shapiro-Wilk test (alpha set at 0.05 with outcome $P > .05$ thereby rejecting the null hypothesis); shoreline data were also judged to be normally distributed by both the Shapiro-Wilk ($P > .05$) and Kolmogorov-Smirnov tests ($P > .1$). After testing for data normalcy, data sets were compared with either one-way ANOVA (parametric test) performed for regional analysis when comparing the absolute values of signal frequencies among the infarct, PIZ and RA, while a paired *t*-test (parametric test) was used to compare signal frequencies in the PIZ and RA normalized against the infarct from the same microscopic slide. An unpaired *t*-test was used to compare the 3-Cl-Tyr:Tyr ratios, total thiol levels and echocardiogram parameters from the sham and AMI groups. Linear regression was used for all shoreline analysis. In all cases $P < .05$ was considered to be statistically significant.

ACKNOWLEDGEMENT

The authors acknowledge the facilities and the scientific and technical assistance of Microscopy Australia at the Australian Centre for Microscopy & Microanalysis at the University of Sydney. Open access publishing facilitated by The University of Sydney, as part of the Wiley - The University of Sydney agreement via the Council of Australian University Librarians.

CONFLICT OF INTEREST

None of the authors have conflicts to declare.

AUTHOR CONTRIBUTIONS

PKW, HS and NJCK did conceptualization. HS, MEK, YL, AG, ALS, SV and CvR did methodology. HS, PAY and CvR


performed formal analysis. HS, MEK, ALS and GA did investigation. HS and PKW did data curation. BSR, SV, HS and MEK contributed curating specimens and storage. HS and PKW wrote—original draft preparation. HS, MEK, YL, BSR, NJCK and PKW wrote—Review & Editing. PKW and BSR did supervision.

DATA AVAILABILITY STATEMENT

The data that support the findings of this study are available from the corresponding author upon reasonable request.

ORCID

Sally Vuong  <https://orcid.org/0000-0003-2295-7893>

Nicholas J. C. King  <https://orcid.org/0000-0002-3877-9772>

[org/0000-0002-3877-9772](https://orcid.org/0000-0002-3877-9772)

Paul K. Witting  <https://orcid.org/0000-0003-2237-7004>

REFERENCES

- Sanchis-Gomar F, Perez-Quilis C, Leischik R, Lucia A. Epidemiology of coronary heart disease and acute coronary syndrome. *Ann Transl Med.* 2016;4(13):256.
- Neuzil J, Rayner BS, Lowe HC, Witting PK. Oxidative stress in myocardial ischaemia reperfusion injury: a renewed focus on a long-standing area of heart research. *Redox Rep.* 2005;10(4):187-197.
- Kalogeris T, Baines CP, Krenz M, Korthuis RJ. Cell biology of ischemia/reperfusion injury. *Int Rev Cell Mol Biol.* 2012;298:229-317.
- Vinten-Johansen J. Involvement of neutrophils in the pathogenesis of lethal myocardial reperfusion injury. *Cardiovasc Res.* 2004;61(3):481-497.
- Zhao ZQ, Nakamura M, Wang NP, et al. Dynamic progression of contractile and endothelial dysfunction and infarct extension in the late phase of reperfusion. *J Surg Res.* 2000;94(2):133-144.
- Vasilyev N, Williams T, Brennan ML, et al. Myeloperoxidase-generated oxidants modulate left ventricular remodeling but not infarct size after myocardial infarction. *Circulation.* 2005;112(18):2812-2820.
- Ali M, Pulli B, Courties G, et al. Myeloperoxidase inhibition improves ventricular function and remodeling after experimental myocardial infarction. *JACC Basic Transl Sci.* 2016;1(7):633-643.
- Mollenhauer M, Friedrichs K, Lange M, et al. Myeloperoxidase mediates postischemic arrhythmic ventricular remodeling. *Circ Res.* 2017;121(1):56-70.
- Albertine KH, Weyrich AS, Ma XL, Lefer DJ, Becker LC, Lefer AM. Quantification of neutrophil migration following myocardial ischemia and reperfusion in cats and dogs. *J Leukoc Biol.* 1994;55(5):557-566.
- Andreadou I, Cabrera-Fuentes HA, Devaux Y, et al. Immune cells as targets for cardioprotection: new players and novel therapeutic opportunities. *Cardiovasc Res.* 2019;115(7):1117-1130.
- Chang Q, Ornatsky OI, Siddiqui I, Loboda A, Baranov VI, Hedley DW. Imaging mass cytometry. *Cytometry A.* 2017;91(2):160-169.
- Rehg JE, Bush D, Ward JM. The utility of immunohistochemistry for the identification of hematopoietic and lymphoid cells in normal tissues and interpretation of proliferative and inflammatory lesions of mice and rats. *Toxicol Pathol.* 2012;40(2):345-374.
- Jordan JE, Zhao ZQ, Vinten-Johansen J. The role of neutrophils in myocardial ischemia-reperfusion injury. *Cardiovasc Res.* 1999;43(4):860-878.
- Koide S-I, Kugiyama K, Sugiyama S, et al. Association of polymorphism in glutamate-cysteine ligase catalytic subunit gene with coronary vasomotor dysfunction and myocardial infarction. *J Am Coll Cardiol.* 2003;41(4):539-545.
- Kudoh K, Uchinami H, Yoshioka M, Seki E, Yamamoto Y. Nrf2 activation protects the liver from ischemia/reperfusion injury in mice. *Ann Surg.* 2014;260(1):118-127.
- Sugden PH, Clerk A. "Stress-responsive" mitogen-activated protein kinases (c-Jun N-terminal kinases and p38 mitogen-activated protein kinases) in the myocardium. *Circ Res.* 1998;83(4):345-352.
- Xu B, Zhang J, Strom J, Lee S, Chen QM. Myocardial ischemic reperfusion induces de novo Nrf2 protein translation. *Biochim Biophys Acta.* 2014;1842(9):1638-1647.
- Yeh C-C, Li H, Malhotra D, et al. Distinctive ERK and p38 signaling in remote and infarcted myocardium during post-MI remodeling in the mouse. *J Cell Biochem.* 2010;109(6):1185-1191.
- Hamid T, Guo SZ, Kingery JR, Xiang X, Dawn B, Prabhu SD. Cardiomyocyte NF-kappaB p65 promotes adverse remodeling, apoptosis, and endoplasmic reticulum stress in heart failure. *Cardiovasc Res.* 2011;89(1):129-138.
- Kettle AJ, Winterbourn CC. Myeloperoxidase: a key regulator of neutrophil oxidant production. *Redox Rep.* 1997;3(1):3-15.
- Davies MJ. Protein oxidation and peroxidation. *Biochem J.* 2016;473(7):805-825.
- Winterbourn CC. Reconciling the chemistry and biology of reactive oxygen species. *Nat Chem Biol.* 2008;4(5):278-286.
- Lee PJ, Jiang B-H, Chin BY, et al. Hypoxia-inducible factor-1 mediates transcriptional activation of the heme oxygenase-1 gene in response to hypoxia. *J Biol Chem.* 1997;272(9):5375-5381.
- Barancik M, Htun P, Strohm C, Kilian S, Schaper W. Inhibition of the cardiac p38-MAPK pathway by SB203580 delays ischemic cell death. *J Cardiovasc Pharmacol.* 2000;35(3):474-483.
- Nagarkatti DS, Sha'afi RI. Role of p38 MAP kinase in myocardial stress. *J Mol Cell Cardiol.* 1998;30(8):1651-1664.
- Litt MR, Jeremy RW, Weisman HF, Winkelstein JA, Becker LC. Neutrophil depletion limited to reperfusion reduces myocardial infarct size after 90 minutes of ischemia. Evidence for neutrophil-mediated reperfusion injury. *Circulation.* 1989;80(6):1816-1827.
- El Kazzi M, Shi H, Vuong S, et al. Nitroxides mitigate neutrophil-mediated damage to the myocardium after experimental myocardial infarction in rats. *Int J Mol Sci.* 2020;21(20):7650.
- Wang XS, Kim HB, Szuchman-Sapir A, McMahon A, Dennis JM, Witting PK. Neutrophils recruited to the myocardium after acute experimental myocardial infarct generate hypochlorous acid that oxidizes cardiac myoglobin. *Arch Biochem Biophys.* 2016;612:103-114.
- Ključević N, Boban D, Milat AM, et al. Expression of leukocytes following myocardial infarction in rats is modulated by moderate white wine consumption. *Nutrients.* 2019;11(8):1890.
- Chami B, Hossain F, Hambly TW, et al. Serum amyloid A stimulates vascular and renal dysfunction in apolipoprotein E-deficient mice fed a normal chow diet. *Front Immunol.* 2019;10:380.

31. Chami B, Jeong G, Varda A, et al. The nitroxide 4-methoxy TEMPO inhibits neutrophil-stimulated kinase activation in H9c2 cardiomyocytes. *Arch Biochem Biophys*. 2017;629:19-35.
32. Ockaili R, Natarajan R, Salloum F, et al. HIF-1 activation attenuates postischemic myocardial injury: role for heme oxygenase-1 in modulating microvascular chemokine generation. *Am J Physiol Heart Circ Physiol*. 2005;289(2):H542-548.
33. Tecchio C, Micheletti A, Cassatella MA. Neutrophil-derived cytokines: facts beyond expression. *Front Immunol*. 2014;5:508.
34. Klebanoff SJ. Myeloperoxidase: friend and foe. *J Leukoc Biol*. 2005;77(5):598-625.
35. Das DK, Maulik N. Cardiac genomic response following preconditioning stimulus. *Cardiovasc Res*. 2006;70(2):254-263.
36. Wang G, Hamid T, Keith RJ, et al. Cardioprotective and antiapoptotic effects of heme oxygenase-1 in the failing heart. *Circulation*. 2010;121(17):1912-1925.
37. Woods CG, Fu J, Xue P, et al. Dose-dependent transitions in Nrf2-mediated adaptive response and related stress responses to hypochlorous acid in mouse macrophages. *Toxicol Appl Pharmacol*. 2009;238(1):27-36.
38. Wei Y, Liu XM, Peyton KJ, et al. Hypochlorous acid-induced heme oxygenase-1 gene expression promotes human endothelial cell survival. *Am J Physiol Cell Physiol*. 2009;297(4):C907-C915.
39. Yan AT, Shayne AJ, Brown KA, et al. Characterization of the peri-infarct zone by contrast-enhanced cardiac magnetic resonance imaging is a powerful predictor of post-myocardial infarction mortality. *Circulation*. 2006;114(1):32-39.
40. Chen A-H, Arany PR, Huang Y-Y, et al. Low-level laser therapy activates NF-kB via generation of reactive oxygen species in mouse embryonic fibroblasts. *PLoS One*. 2011;6(7):e22453.
41. Mitchell S, Vargas J, Hoffmann A. Signaling via the NFkappaB system. *Wiley Interdiscip Rev Syst Biol Med*. 2016;8(3):227-241.
42. Churg A, Marshall CV, Sin DD, et al. Late intervention with a myeloperoxidase inhibitor stops progression of experimental chronic obstructive pulmonary disease. *Am J Respir Crit Care Med*. 2012;185(1):34-43.
43. Yeoh BS, Aguilera Olvera R, Singh V, et al. Epigallocatechin-3-gallate inhibition of myeloperoxidase and its counter-regulation by dietary iron and lipocalin 2 in murine model of gut inflammation. *Am J Pathol*. 2016;186(4):912-926.
44. Yu G, Liang Y, Huang Z, Jones DW, Pritchard KA Jr, Zhang H. Inhibition of myeloperoxidase oxidant production by N-acetyl lysyltyrosylcysteine amide reduces brain damage in a murine model of stroke. *J Neuroinflammation*. 2016;13(1):119.
45. Bhindi R, Witting PK, McMahon AC, Khachigian LM, Lowe HC. Rat models of myocardial infarction. Pathogenetic insights and clinical relevance. *Thromb Haemost*. 2006;96(5):602-610.
46. Hawkins CL, Morgan PE, Davies MJ. Quantification of protein modification by oxidants. *Free Radic Biol Med*. 2009;46(8):965-988.
47. Shivanandan A, Radenovic A, Sbalzarini IF. MosaicIA: an ImageJ/Fiji plugin for spatial pattern and interaction analysis. *BMC Bioinform*. 2013;14:349.
48. Helmuth JA, Paul G, Sbalzarini IF. Beyond co-localization: inferring spatial interactions between sub-cellular structures from microscopy images. *BMC Bioinform*. 2010;11:372.
49. Rahman I, Kode A, Biswas SK. Assay for quantitative determination of glutathione and glutathione disulfide levels using enzymatic recycling method. *Nat Protoc*. 2006;1(6):3159-3165.

SUPPORTING INFORMATION

Additional supporting information may be found in the online version of the article at the publisher's website.

How to cite this article: Shi H, El Kazzi M, Liu Y, et al. Multiplex analysis of mass imaging data: Application to the pathology of experimental myocardial infarction. *Acta Physiol*. 2022;235:e13790. doi:[10.1111/apha.13790](https://doi.org/10.1111/apha.13790)